Granular Matter (2009) 11:99–113
DOI 10.1007/s10035-009-0125-7

Vibration induced flow in hoppers: continuum and DEM model approaches

Paul A. Langston · Andrew J. Matchett · Feras Y. Fraige · John Dodds

Received: 29 August 2007 / Published online: 7 February 2009

Abstract A 2D and a 3D discrete element model (DEM) simulation of cohesive spherical particles are applied to assess the benefit of point source vibration to induce flow in wedge-shaped hoppers. The model is closely compared with a continuum model based on arch stability. A significant aspect of this study is the scaling of the continuum system to a discrete system of 500 particles in 2D and 2500 particles in 3D. This illustrates how such models can complement each other. The continuum model can cope with a full-scale industrial system, but is complex with significant assumptions. The discrete approach is relatively simple at the particle level with minimal assumptions but computationally demanding. The DEM model supports the basic conclusions of the continuum model. The vibration source must be located at the appropriate height above the outlet on the hopper to optimise its flow enhancement. Too low and stable arches can form above. Too high and it might not break the stable arches in the material below. The passive/active nature of the material during vibration and flow is also illustrated. The DEM model also shows that low frequency high amplitude vibration can enable flow through small orifices.

Keywords Bulk solids · Vibration · DEM · Hoppers · Materials handling · Storage

P. A. Langston (✉)
School of Chemical and Environmental Engineering,
Nottingham University, University Park,
Nottingham NG7 2RD, UK
e-mail: P.Langston@nottingham.ac.uk

A. J. Matchett
Chemical Engineering, University of Teesside,
Middlesbrough TS1 3BA, UK

F. Y. Fraige
Faculty of Mining and Environmental Engineering,
Al-Hussein Bin Talal University Jordan,
P.O. Box 20, Ma'an, Jordan

J. Dodds
Centre RAPSODEE, Ecole Des Mines, Campus Jarland,
81013 Albi, France

1 Introduction

1.1 Background

Processing of granular and powder materials is important in many engineering applications. These encompass operations such as storage, conveying, mixing and sizing from small scale pharmaceutical or food processing operations, where composition control may be critical, to large scale minerals industry storage where wall stress and silo-quake may be important. Bulk solids behaviour is generally more unpredictable than for gases and liquids and problems such as unsteady flows often occur in the course of handling and processing.

The design of hoppers to achieve a smooth and reliable mass flow rate for a specified material has long been a subject of interest to both researchers and process engineers, such as [1–3] and, more recently [4,5]. Although this has been greatly advanced by the introduction of pre-measuring the various flow properties of the material encountered [6], the determination of a range of flow parameters for a bulk solid can be an expensive exercise [7]. Moreover, the classic shear testers often suggest larger hopper outlets than is actually required [2] and most practical design methods are based on theoretical-empirical approaches. Conventional mass-flow hopper design tends to give tall hoppers with steep sides and large outlets. This gives problems in areas of limited space and in conditions where small or modest flowrates are required.

Vibration is often used as a means of initiating and/or controlling flow. It is relatively inexpensive and can be fitted as a "bolt-on" to existing hoppers. However, the mechanics of vibration are complex and there is much confusion as to how vibration actually works [8]. Indeed, in some circumstances, vibration is used to compact and consolidate materials rather than dilate and induce flow. Some workers see vibration as a means of ensuring flow in situations that are on the limit of conventional flow, and of modest effect [9]. Roberts has provided the most complete body of work on the use of vibration in hoppers [10]. He developed a modified, vibrating, Jenike shear cell and a Jenike-type method of analysis. He also reported modest improvements in flow with the application of vibration. Matsusaka was able to get cohesive materials to flow through very small, capillary tubes by use of vibration—well beyond the limits of standard design. [11–13]. Matchett [14] used a continuum approach to model limiting states during the application of vibration to a hopper wall. He assumed a circular arc principal stress orientation, originally proposed by Enstad [2], modified to operate in principal stress space. This provided a rational method for positioning a vibrational device in the hopper and was based upon standard continuum material properties with no need for sophisticated vibrational cells. The model was a pseudo-static, limit analysis with no dynamic terms.

However, other approaches to modelling have developed in recent years. With increasing computer power simulation is becoming important in understanding particulate processing using techniques such as Finite Element or the Discrete Element Method DEM.

1.2 Objectives

This paper uses a DEM technique to investigate the potential for hopper vibration to promote and control flow. The method and results are compared with a continuum Stress Arc Model [14]. Section 2 summarises this continuum model and describes how it shows that the position of the vibration source on a hopper is critical. Section 3 summarises the DEM model and describes how the data was selected to match the continuum model as close as possible. Section 4 shows the results of the DEM simulations. Section 5 summarises the main conclusions and suggestions for further work.

2 Summary of continuum model study

2.1 The wedge, circular arc model

The circular arc model follows the approach of Enstad [2], extended by Matchett [14]. The principal stresses are assumed to aligned in an arc configuration—see Fig. 1. The stress arcs are circular and make a constant angle, β, to the wall normal. β is controlled by the angle of wall friction [14], and limiting values are given by:

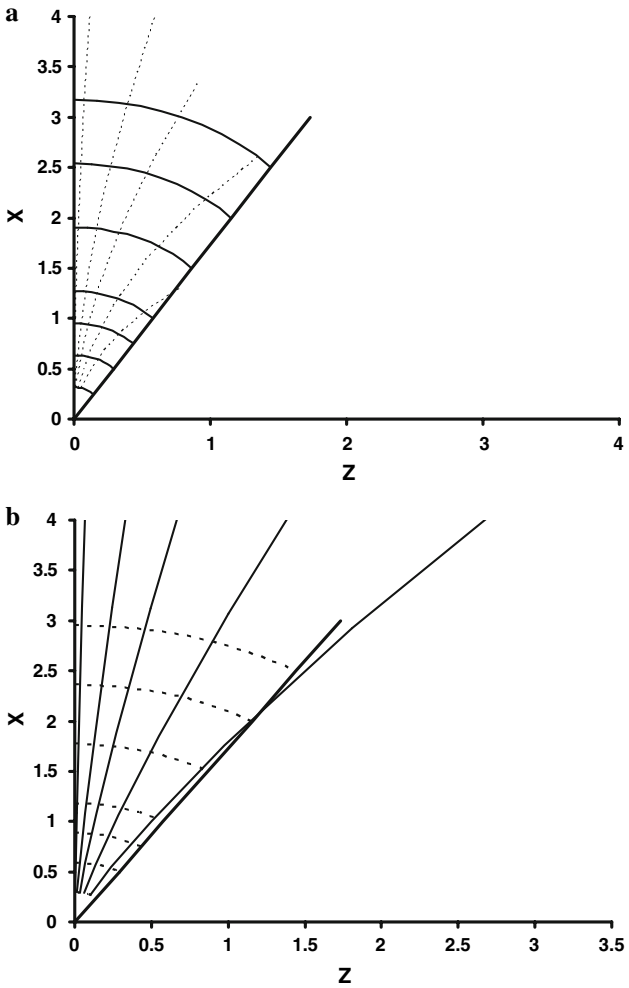

Fig. 1 Principal stress orientation in conditions of limiting passive and active stress (scale in m): **a** passive stress state; **b** active stress state

$$\beta_{\text{passive}} = 0.5\left(\arcsin\left(\frac{\sin\phi_w}{\sin\phi}\right) + \phi_w\right)$$
$$\beta_{\text{active}} = 0.5\left(\arcsin\left(\frac{\sin\phi_w}{\sin\phi}\right) - \phi_w\right) \quad (1)$$

The radial stress, averaged over the area of an arc is S (Pa), and there is an arc stress E (Pa) acting azimuthally at the point where the arc meets the wall–Fig. 2. The major principal stress is shown by the thick lines in Fig. 1. Figure 1a shows the passive case, where E is the major principal stress, with the thicker lines orientated as circular arcs across the vessel. Figure 1b shows the active case. S is the major principal stress and acts down the vessel.

The basis of the model is shown in Fig. 2. The model presented is a 1D model, in terms of average radial stress S. It is a plane stress model and stresses in the third dimension are assumed to have no effects upon the system. Thus, the

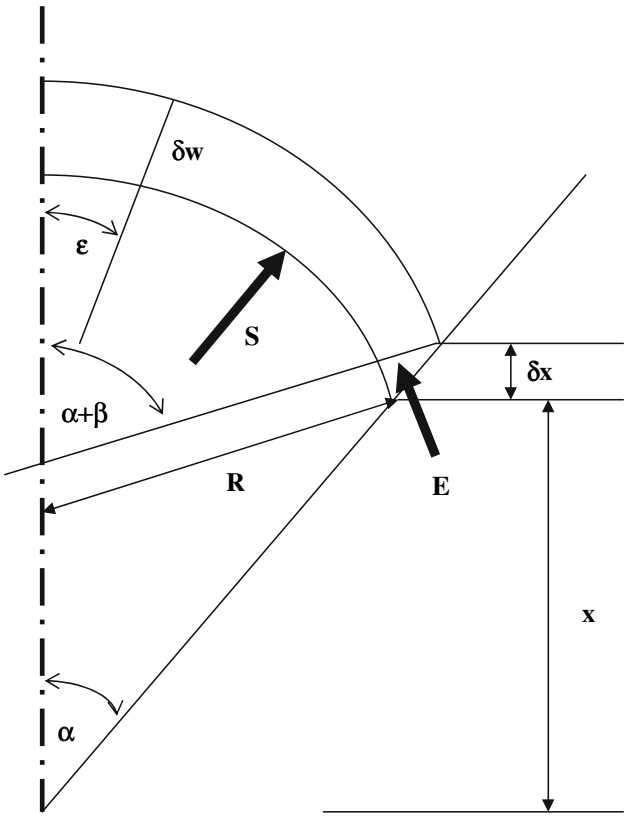

Fig. 2 The 1D, circular arc model of stresses within bulk solids in wedge hoppers

model derived is for one unit depth in the third dimension. The position of an arc is located by the vertical distance from the apex of the wedge, of half-angle α, to the point where the arc cuts the wall: x (m). At height x, the arc has radius R (m), and it can be shown that:

$$R = x\frac{\tan\alpha}{\sin(\alpha+\beta)} = a_1 x \tag{2}$$

Consider an incremental element between x and $x+\delta x$—Fig. 2. The volume of the incremental element, described by circular arcs at x and $x+\delta x$, between the centre-line and the wall is δV. The thickness of the element, δw (m), is shown at angle to the vertical ε in Fig. 2. δw is a function of ε, and it can be shown [14] that:

$$\begin{aligned}\frac{\partial w}{\partial x} &= a_1 + a_2\cos\varepsilon\\ a_2 &= 1 - a_1\cos(\alpha+\beta)\end{aligned} \tag{3}$$

Thus, the volume of the incremental element, Fig. 2, is given by:

$$\delta V = \frac{\partial V}{\partial x}\delta x = \int_0^{\alpha+\beta} R\frac{\partial w}{\partial x}\delta x\, d\varepsilon = \int_0^{\alpha+\beta} R\,(a_1 + a_2\cos\varepsilon)\,\delta x\, d\varepsilon \tag{4}$$

Hence:

$$\delta V = R\,(a_1(\alpha+\beta) + a_2\sin(\alpha+\beta))\,\delta x \tag{5}$$

At the wall, stress E acts upon area $\frac{\partial w}{\partial x}\delta x$ at $\varepsilon = \alpha+\beta$:

$$\frac{\partial w}{\partial x}(\alpha+\beta) = \frac{\cos\beta}{\cos\alpha} \tag{6}$$

Thus, a vertical force balance on the half wedge, incremental element at incipient flow or steady state, with no inertial terms, gives:

$$\begin{aligned}&[SR\sin(\alpha+\beta)]_x - [SR\sin(\alpha+\beta)]_{x+\delta x}\\ &\quad -\left(\frac{\partial V}{\partial x}\right)\delta x\rho g + E\frac{\cos\beta}{\cos\alpha}\delta x\sin(\alpha+\beta) = 0\end{aligned} \tag{7}$$

which gives the differential equation:

$$\begin{aligned}-\frac{d}{dx}[SR\sin(\alpha+\beta)] - \rho g\frac{\partial V}{\partial x} + E\frac{\cos\beta\sin(\alpha+\beta)}{\cos\alpha} &= 0\\ \frac{d}{dx}[SR] = -\frac{\rho g R\{a_1(\alpha+\beta)+a_2\sin(\alpha+\beta)\}}{\sin(\alpha+\beta)} + E\frac{\cos\beta}{\cos\alpha}&\end{aligned} \tag{8}$$

It is assumed that azimuthal stress E is related to radial stress S by a Mohr–Coulomb type of relationship [14]:

$$E = JS + (J-1)T \tag{9}$$

Where

$$\begin{aligned}\tau &= \sigma\tan\phi + c\\ T &= c/\tan\phi\\ J_{\text{passive}} &= \frac{1+\sin\phi}{1-\sin\phi}\\ J_{\text{active}} &= \frac{1-\sin\phi}{1+\sin\phi}\end{aligned} \tag{10}$$

ϕ is the angle of the yield locus and T is the cohesive stress for the linearised yield locus. At yield $J = J_{\text{passive}}$ or J_{active}, but in the general case, J could take values between these two limits. This study will be limited to the yield conditions. E and S and principal stresses, thus, they are related to τ and σ via the Mohr-circle stress relationships:

$$\begin{aligned}p' &= \frac{E+S}{2} + T\\ q' &= \frac{E-S}{2}\\ \tau &= q'\sin 2\phi\\ (\sigma+T) &= \sigma' = p' + q'\cos 2\phi\end{aligned} \tag{11}$$

Substitution for E in terms of S with boundary condition:

$$x = H : S = S^*$$

gives the explicit equation for S:

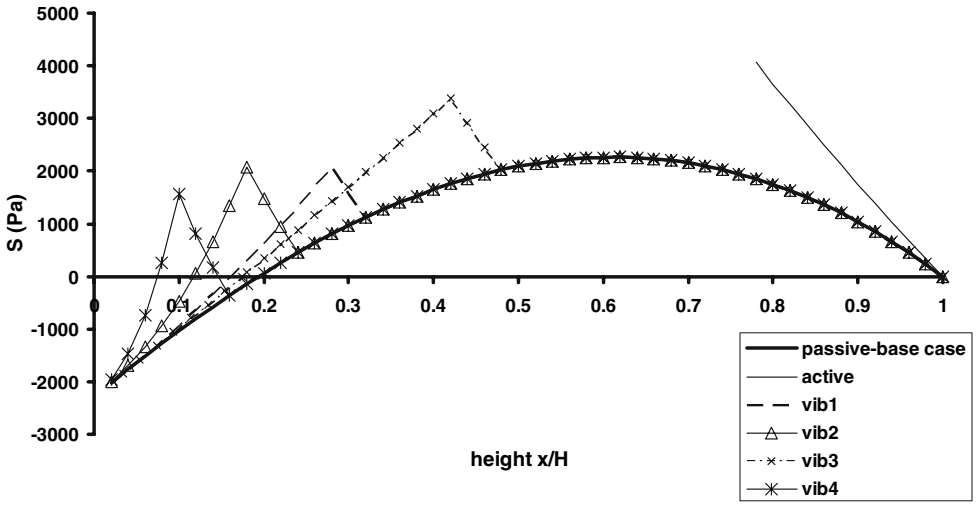

Fig. 3 Typical stress distributions for average radial stress S; 45° wedge hopper; $\phi = 28°$; $\phi_w = 17°$; $T = 2,500$ Pa

$$S = \left(\frac{A_3 x}{A_1 - 1}\right)\left\{1 - \left(\frac{x}{H}\right)^{(A_1-1)}\right\} - \frac{A_2}{A_1}\left\{1 - \left(\frac{x}{H}\right)^{A_1}\right\} + S^*\left(\frac{x}{H}\right)^{A_1}$$

$$A_1 = \frac{J\cos\beta}{a_1\cos\alpha} - 1 \qquad (12)$$

$$A_2 = \frac{\cos\beta(J-1)T}{a_1\cos\alpha}$$

$$A_3 = \rho g\left(\frac{a_1(\alpha+\beta) + a_2\sin(\alpha+\beta)}{\sin(\alpha+\beta)}\right)$$

This equation is of the same form as the well-known Walker/Walters/Enstad equations for stress distribution [2, 15,16].

2.2 Properties of the model subject to vibration

The properties of the model have been explained in detail with respect to a conical hopper by Matchett [14], but a brief resume with respect to 2D wedge hoppers will be given here.

Typical stress distributions are shown in Fig. 3. During flow, or incipient flow, it is assumed that the material will be in the passive mode throughout the vessel with the material at yield ($J = J_{\text{passive}}$) and the value of β at its maximum for the passive stress state. This is the base case in Fig. 3. The stress takes on a typical Walker shape, increasing, passing through a maximum and then decreasing. At some point, it crosses the S axis and goes into tension. This gives a simple flow rule—if the wedge is truncated at a point where S is positive, and the bottom removed, then flow will take place. Hence the critical outlet dimension can be readily found. If S is negative at the point of truncation, then the material will relax away from the yield locus and a stable, cohesive arch will form.

For an active stress state throughout, $J = J_{\text{active}}$ and β takes the value appropriate to the active case. For this situation, S increases continuously down the vessel. Hence, flow would take place for truncation of the wedge at any reasonable value of x.

Table 1 Continuum model critical outlet dimensions: minimum values if x (normalised) and outlet size consistent with material flow

	x m/m	Outlet m/m	Vibrated section From	To
Active	0	0		
Passive	0.193	0.386	none	
vib1	0.16	0.32	0.26	0.3
vib2	0.118	0.236	0.18	0.2
vib3	0.174	0.348	0.42	0.46
vib4	0.193	0.386	0.1	0.14

It is proposed that vibration is applied, causing motion of the wall in a given section of the wedge. At the limits of compression, the material is in the passive stress state. However, during the expansion part of the vibration cycle, the material will tend to the active state, and in the limit reach an active stress state. Thus, the model can predict limiting conditions of stress with applied vibration. A spreadsheet has been devised which predicts the value of S down the wedge, but the state of stress can be changed in any section, using the final value in the section above as boundary conditions for the new stress state.

Four vibration scenarios are shown in Fig. 3: vib1; vib2; vib3, vib4 with critical outlet properties shown in Table 1. In all cases, stress S rises through the expanded cycle of the vibrated section. However, that increased stress is quickly dissipated against wall friction in the subsequent, passive section of the cone. Figure 3, vib1 shows that applied vibration can induce flow through a smaller outlet than the base case. Figure 3, vib2 shows that with optimal selection of the vibration device then the decrease in allowable outlet dimension can be very significant. However, Fig. 3, vib3 and vib4

shows that inappropriate selection of location of the vibration device can result in little effect upon the outlet dimension. The vibrator is above the location of the critical arch in vib3. The same effect occurs when the vibration device is mounted below the critical arch location—vib4.

From these observations, the key features of the circular arc model can be deduced:

- The expansion part of the vibration cycle is assumed to induce an active stress state within the material, resulting in an increase in stress throughout the vibrated section. If an active stress state can be induced, then flow may take place out of much smaller outlets than for the unvibrated state.
- In the compressive phase of the vibration cycle, the material is assumed to be in the passive stress state, and flow may cease. Thus flow may be "stick-slip".
- Thus, lines of principal stress orientation can be identified for the limiting states of active and passive stress–Fig. 1. During vibration, the stress orientation should oscillate between these two liming modes.
- Location of the vibration device is critical for successful flow—if the source of vibration is mounted too high or too low within the wedge, then it has a negligible effect upon the critical outlet for flow.
- The location of the critical arch and hence optimum position for applying vibration can, in principle, be calculated from the model and material properties

In the general case, the state of stress within the material is not known—is it fully plasticised or within the elastic range? However, this is a limit analysis. The material is undergoing compression in the compressive part of the vibration cycle, and if the amplitude is sufficient this will induce a state of passive yield. Therefore, the assumption is justified in this context, as it is in all limit analysis [2,14,15]. Thus, it is possible to locate the region for optimum application of vibration.

The Mohr–Coulomb yield criterion gives a good estimate of the stresses. It is more problematic to estimate the required amplitude to achieve flow, and it should be noted that flow could also be induced in sub-yield conditions if the relaxation of vertical forces is sufficient to cause a net downward force. The model cannot predict resonance and frequency related effects. Hence a comparison with the DEM is potentially useful.

3 DEM simulation

3.1 Particle flow model

The DEM technique uses an explicit time stepping approach to numerically integrate the motion of each particle from the resulting forces acting on them at each timestep. The particle flow model here follows a fairly standard DEM approach for spheres. Cohesion is also included here. The inter-particle and particle wall contacts are modelled using the spring–dashpot–slider analogy. Contact forces are modelled in the normal and tangential directions with respect to the line connecting the particles centres. The normal component, F_n, is expressed as:

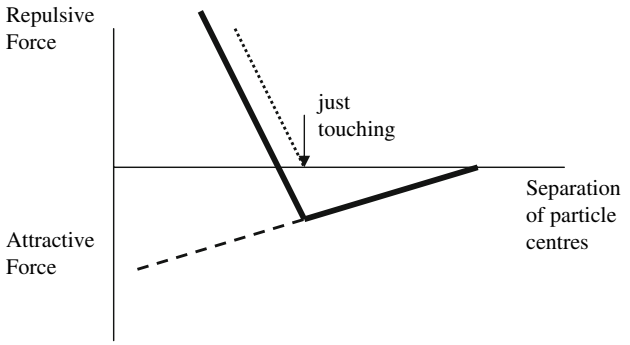

Fig. 4 Particle normal contact force model; shows cohesive (*dashed*) and repulsive components (*dotted*), and net force (*thicker line*)

$$F_n = k_n \delta_n - k_{na} \delta_{na} - c_n v_n \tag{13}$$

The first term on the right is the elastic force in the normal direction, F_{ne}, modelled using Hooke's law where, k_n is the stiffness in the normal direction and δ_n is the displacement. The second term is the attractive cohesive force represented by a stiffness k_{na} and an overlap δ_{na} of the attractive fields. The third term is the normal contact damping, where, c_n is the normal damping constant, and v_n is the normal relative velocity between the contacted objects. The first two terms are illustrated in Fig. 4.

The tangential component, F_t, is given by:

$$F_t = F_f - c_t v_t \tag{14}$$

where F_f is the friction force and the other term is the damping force in the tangential direction. The tangential damping component is modelled in a similar way to the normal damping but with different damping constant, c_t, and the tangential component of the relative velocity, v_t. In this model, only the normal damping force is incorporated because the tangential component is relatively small.

The friction force is modelled to represent elastic and plastic deformation components. The modelling of friction may be related to the two known types of friction: prior to gross sliding and at or after sliding. The first case is modeled using Hooke's law as in the normal direction and it can be given by:

$$F_{fb} = k_t \delta_t \tag{15}$$

where k_t is the tangential stiffness, and δ_t is the total tangential deformation between the surfaces since their initial

contact. The second case, where the tangential deformation exceeds the Coulomb frictional limit, is when gross sliding occurs. There is no further increase in particle tangential deformation and the friction force at or after gross sliding is given by:

$$F_{fa} = \mu F_{ne} \tag{16}$$

where μ is the coefficient of friction and F_{ne} is the normal elastic force.

The model uses a half step leap-frog Verlet numerical integration scheme to update particle positions and velocities. A zoning method is used to increase the computational efficiency of determining particle contacts. A more detailed description of the particle model is found in [17,18]. The modelling techniques have undergone detailed quantified experimental validation in 2D and 3D for large non-cohesive particles, including spherical particles, sphero-discs and cubes, see for example [19,20]. This paper concentrates on comparing features of a detailed continuum approach with the discrete approach. The results are compared in a qualitative manner.

3.2 Scaling simulations and data in 2D

For ease of presentation and to reduce the CPU requirements on the large number of simulations required here our 3D model of spherical particles was initially restricted to 2D. That is translational motion in the z, x (vertical) axes and rotation about the y-axis. The next question is what particle size should be used for a reasonable comparison with the Stress Arc continuum model? An arbitrary small size of 90–100 μm (normal distribution) was chosen. These are small enough for cohesion. There may also be some air drag effects at this size but these would be less significant than the cohesion. The obvious limitation of DEM is the computational CPU requirement. The number of particles in the 2D simulations is 500 which obviously implies a very small hopper, but this is large enough to test the principles of the physics and compare with the continuum model. Many discrete particle simulations use periodic boundaries but these would not be useful here. It may be possible to model a "larger system" by only modelling the region near to the hopper outlet and impose an "overburden load" on the top particles, but the results here are reasonable without this.

The particle elastic stiffness was taken as a value that prevented significant overlap between the particles but allowed a reasonable timestep. This is a controversial area of DEM. This has worked well in previous hopper flow simulations where the discharge rate, flow patterns, erratic flow on smaller orifices, blocked flow and stresses agreed well with experimental data and theoretical models, [4,19,20]. However, this does not imply that it will be valid in all situations. The modeller must consider the specific situation. The cohesive stiffness was chosen to give a cohesive force between particles that is comparable with scaled colloidal forces measured by Atomic Force Microscopy [21]. Only particle-particle cohesion was modelled, it was assumed there is no wall adhesion. The coefficient of friction was set to the same value as the continuum model and a typical value of contact damping was used here (both particle-particle and particle-wall) to give moderate restitution coefficients.

Figure 5 shows an example simulation of the hopper. The hopper half-angle was set the same as in the continuum model in Sect. 2 and trial runs undertaken to gauge the orifice size B where arching and blockage occurs. Vibration was imposed by means of two fixed circles which oscillate in size as shown in the figure. These are positioned such that at their smallest size they are just touching the wall at a specified height h above the orifice. The scenario modelled is: hopper filling and settling to time $t = 0.05$ s; open orifice and wait until $t = 0.1$ s to see if there is any flow; start vibration and simulate until $t = 0.4$ s. A small amplitude of vibration was used to represent localised vibration. Note that no vibration is imparted along the walls. Table 2 summarises the principal data used in the simulation. In practice air drag during filling would reduce particle velocities significantly but the filling process is not the critical part of this study.

3.3 Scaling simulations and data in 3D

Despite the advantages of 2D simulation described above, a number of questions can be asked regarding its validity. In a macroscopic approach it is reasonable to assume planar stress for a wedge hopper, but can this be done at the microscopic (particle) level? Particles must "climb over each other" in the same plane and not take the path of minimum energy. This can cause higher dilatancy and higher friction. This could be significant for the critical stress state.

It is well-recognised by the authors that 2D and 3D models have some fundamental differences, however, in this initial, essentially qualitative study, 2D simulations do give some useful insight. [4,22] compare 2D and 3D results in previous DEM hopper flow studies, illustrating similar trends. Further simulations have been undertaken here with a 3D wedge hopper. The principal data is shown in Table 3. The vibrators here are cylinders with length equal to hopper depth in the y-dimension. (x and z dimensions are as per the 2D simulation.) Alternatives would be to use periodic boundaries or frictionless walls in the 3rd dimension to replicate a larger slice in this dimension.

In summary it is important to appreciate that DEM has inherent many simplifications. Some DEM models use variations on the theme such as including rolling friction [23] and periodic boundaries. It is judged that the model here serves its

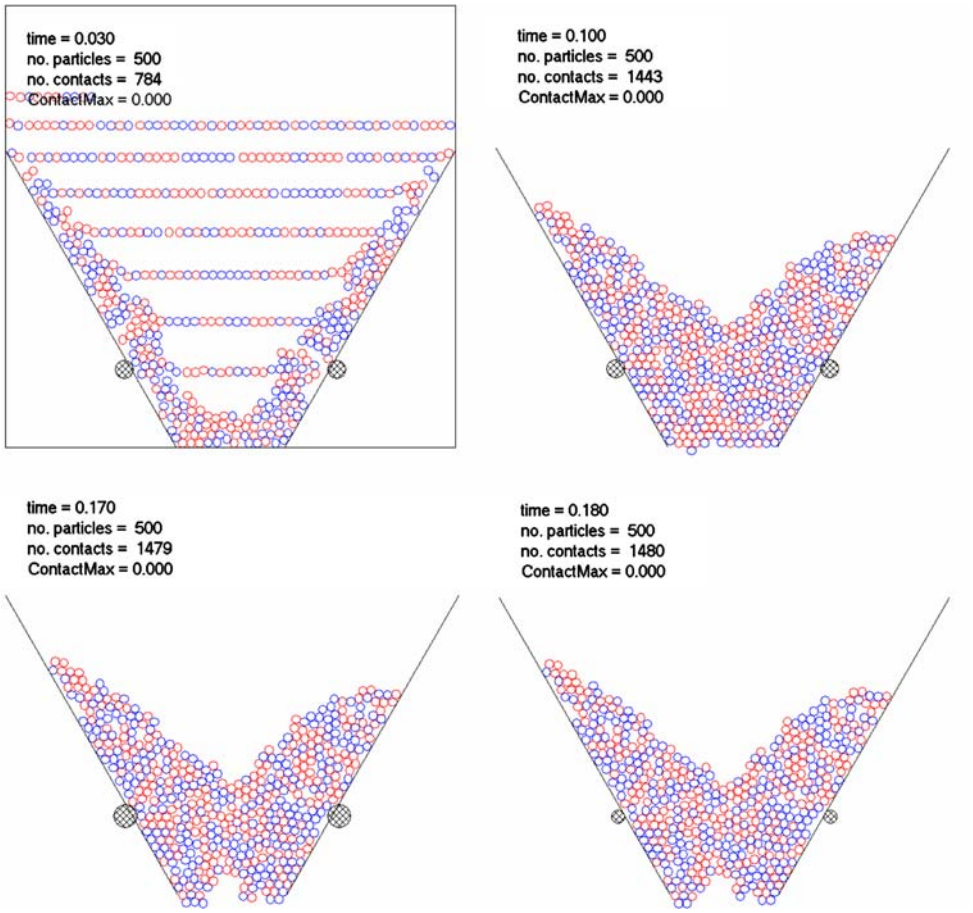

Fig. 5 Two-dimensional simulation scenario: hopper fill, particles added in rows, and settle to $t = 0.05$ s; orifice open and allow time for discharge to $t = 0.1$ s (no discharge here); start vibration and continue till $t = 0.4$ s; shows varying size of vibrator circles. This case is for: $B = 12D$, $h = 9D$, $f = 60$ Hz (just below f_{crit}). Note that there is only one type of particle but two colours, randomly assigned, have been used to help show the pattern of flow (ContactMax records maximum normal contact displacement to 3 d.p. as a check for instabilities in the model)

Table 2 Principal data in 2D DEM simulation

Hopper half-angle, α (°)	30
Orifice size, B (cm, D)	Up to 0.018 ($18D$)
Number of particles	500
Particles diameter range, d (cm)	0.009–0.01
Particle stiffness (dyne/cm)	10,000
Particle cohesive stiffness (dyne/cm)	250
Particle cohesive radius	0.01 Particle radius
Particle coefficient of friction	0.53
Normal damping coefficient (dyne s/cm)	0.05
Particle density (g/cm^3)	0.9
Vibrator radius, R_{vib}	1 D and variation
Vibration amplitude, A	0.3D and variation
Vibration frequency, f (Hz)	10–150
Time step (μs)	1

D is maximum particle diameter
Normal distribution for d
Typical colloidal particle force measured with Atomic Force Microscopy^r is 7.6e-5 dyne for $d = 8$ µm. Assuming surface forces scale as d^2 then 0.01 cm particle gives 0.011 dyne. This was used to set above cohesion data

Table 3 Principal data in 3D DEM simulation (where different to 2D)

Hopper depth (in y)	0.05 and 0.10 (5, 10D)
Orifice size, B (cm, D)	0.012 (12D)
Number of particles	2,500 and 5,000
Particles diameter range, d (cm)	As 2D
Particle stiffness (dyne/cm)	As 2D
Particle cohesive stiffness (dyne/cm)	90 and variation
Particle cohesive radius	As 2D
Particle coefficient of friction	As 2D
Normal damping coefficient (dyne s/cm)	As 2D
Particle density (g/cm^3)	As 2D
Vibrator radius, R_{vib}	1D
Vibration amplitude, A	0.3D
Vibration frequency, f (Hz)	70 and variation
Time step (μs)	As 2D
Time orifice open (s)	0.15 and variation
Time vibration start (s)	0.20 and variation

purpose without these features. DEM is still "some way off" an exact match of real small industrial particles, for example in shape, interstitial air, cohesion and breakage effects. However, the approach is a useful tool to aid understanding. Future studies will investigate the effects of particle shape in vibration which is likely to be the most significant simplification here. It is also emphasised that the timestep here is "quite small" because the particles are "small compared with many DEM studies".

Table 4 Summary of critical frequency f_{crit} results (in Hz) for hoppers in sect. 4.1

B\$h(D)$	0	3	6	9	12
18	0				
14	60–70, c65	10–25, c15	40–50	0	
12	∞(90)	60–70	60–70	60–70	∞(90)
10	∞(150)	∞(150)	60–65	∞(150)	

B is orifice size, h is position height of vibration, in max particle diameters D
∞ highest value tried shown in brackets—no significant discharge
If a range is shown, lowest value had no significant discharge, highest total discharge
If circa shown then the particles discharged but significantly slower than for higher f

4 DEM results

4.1 Critical frequency f_{crit} in 2D

Some preliminary simulations were undertaken to gauge appropriate values of some of the parameters in Table 2 such as timestep. Then runs were undertaken to gauge the orifice size below which material did not readily flow out under gravity. This was about $18D$. For non-cohesive particles the limit is normally about $6D$ [24]. A series of simulations were then undertaken for smaller orifices to determine the critical frequency of vibration required to promote flow at different vibration positions. A summary of the results is shown in Table 4.

The results show general agreement with the conclusions of the continuum model summarised in Sect. 2. If the vibration source is positioned too near the orifice it is not at maximum effectiveness and similarly if it is positioned too high. For $B = 10D$, the smallest case tried here, there is clearly a small region at about $h = 6D$ for vibration to enable complete discharge. Increasing the orifice to $12D$ extends the region, but again if too low or high there is not complete discharge. The frequency required when h is within the flow region seems to be fairly constant, although the exact value of f_{crit} is difficult to gauge. The results for $B = 14D$ are interesting. They have been rerun to check. For a large h the particles discharge without vibration, but at lower h it appears as if the vibrators, which protrude into the hopper at their mid-size, prevent the discharge. The relationship between h and f_{crit} is more complex in this region. The particles are probably on the point of flow for this orifice size and there may be something of a stochastic nature here.

Some examples of these cases are illustrated in the following figures. They show the particle positions (one particle type but two colours are used to help show flow patterns) and also scaled particle contact force vectors (elastic, friction and damping combined but excluding cohesion for clarity). All DEM figures in this paper have the same scaling. The contact force vector maps are shown to give an indication of the nature of the stress. It does not give the direction of the principal stresses directly, but where the largest contact forces are near horizontal the material is tending to the passive state, and where near vertical it is more active. Some of the figures described below show examples of this and some show that the situation is more complex.

Figure 6 shows examples for $B = 10D$ and $h = 6D$ the only h value where total discharge occurred. Figure 6a is for $f = 60$ Hz, which showed little flow, and Fig 6b for $f = 65$ Hz, which showed total discharge. The particle positions and force patterns reveal how the vibration puts the material in passive mode where the major principal stress is near horizontal and this is just able to break the arches and hence enable flow. Figure 6b shows for the material in flow, a more passive state at the vibrators, a more active state above and a dissipated structure below. This is supportive of the assumptions made in Sect. 2 for the Stress Arc continuum model–Fig. 3, for example, the continuum model; would display active stress orientations in the expansive part of the vibration cycle in the region of applied vibration, but passive elsewhere. Figure 7 shows an example for $B = 12D$, $h = 0$, $f = 90$ Hz for which h was too low for discharge and Fig. 8 for $B = 12D$, $h = 12D$, $f = 90$ Hz for which h was too high. These figures illustrate how the vibration has to be carefully located. In essence if it is positioned too low a stable arch forms above the vibration and if too high the arch forms below. Of course vibration sources could be placed at several locations but this would be more complex and more expensive.

An important distinction between the two types of models here is that the continuum model is a limiting case analysis, it does not include inertia. The DEM model is dynamic and includes inertia; hence it can model the effects of frequency in the vibration. This could be important in a situation liable to stick-slip flow. With a large enough frequency the inertial terms are sufficient to maintain motion in the compression part of the cycle and hence maintain flow.

4.2 Critical frequency f_{crit} in 3D

Some preliminary simulations were undertaken to gauge appropriate values of some of the parameters in Table 3 in order to compare with key cases in Sect. 4.1. The hopper depth, $W = 5D$, has been kept fairly small to limit the number of particles, however, this is considered large enough to allow genuine 3D motion. (A further run was undertaken with $W = 5D$.) The main difference with the 3D model is that the material is "more cohesive". This is probably mainly due to the increased co-ordination number (mean number of contacts made by a particle). For close packing systems the maximum is about 6 in 2D and 12 in 3D. The particle mass is

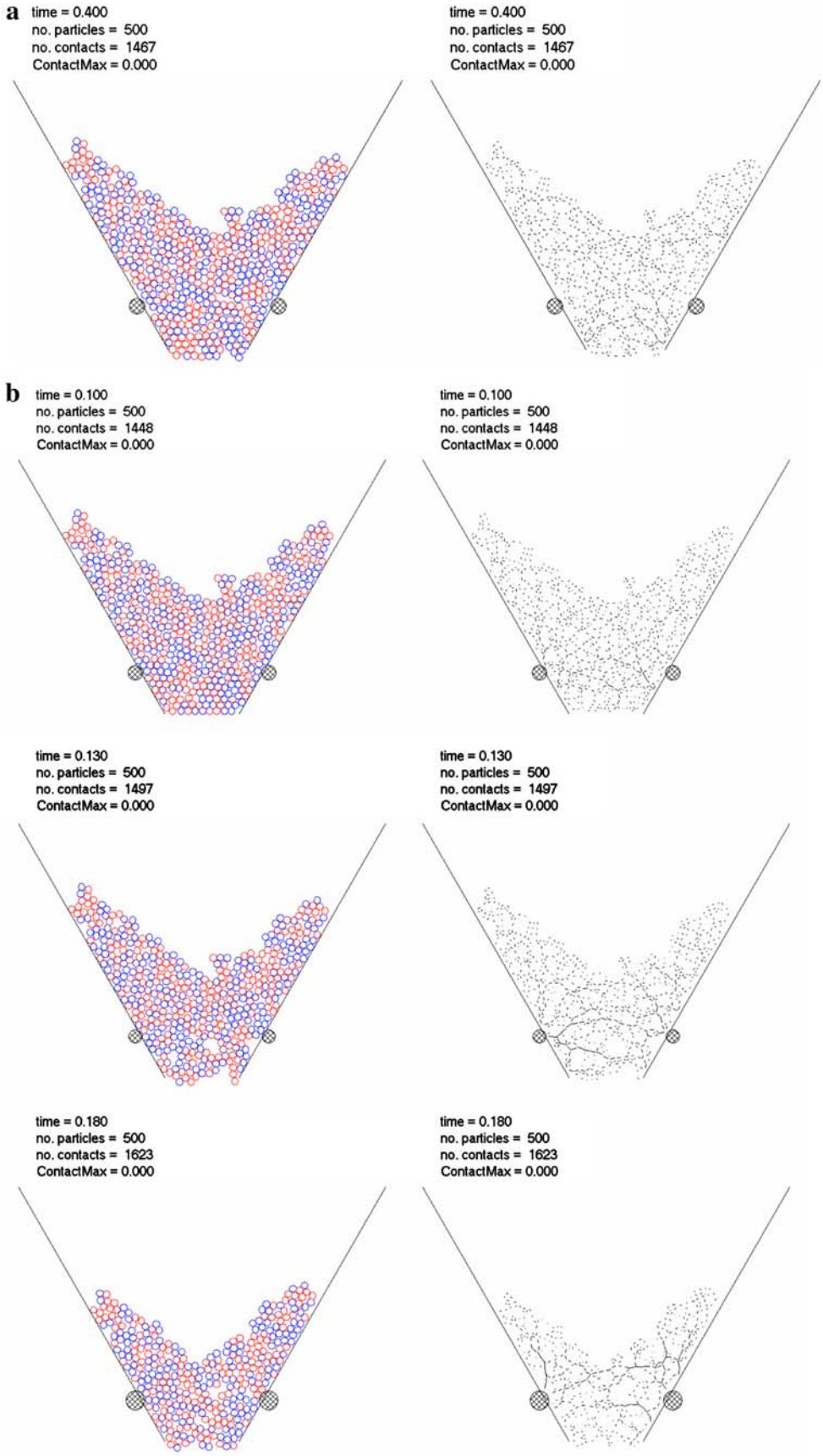

Fig. 6 **a** Two-dimensional simulation: particle positions and normal contact forces at end of simulation for $B = 10D$, $h = 6D$, $f = 60$ Hz, just below f_{crit}; **b** 2D simulation: snapshots of particle positions and contact forces for $B = 10D$, $h = 6D$, $f = 65$ Hz, just above f_{crit}—total discharge at $t = 0.23$ s

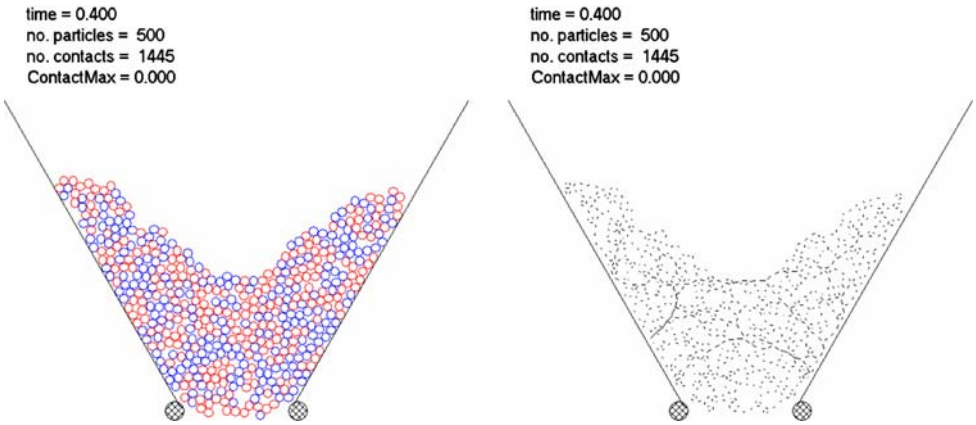

Fig. 7 Two-dimensional simulation: particle positions and contact forces at end of simulation for $B = 12D$, $h = 0$, $f = 90$ Hz, showing negligible discharge

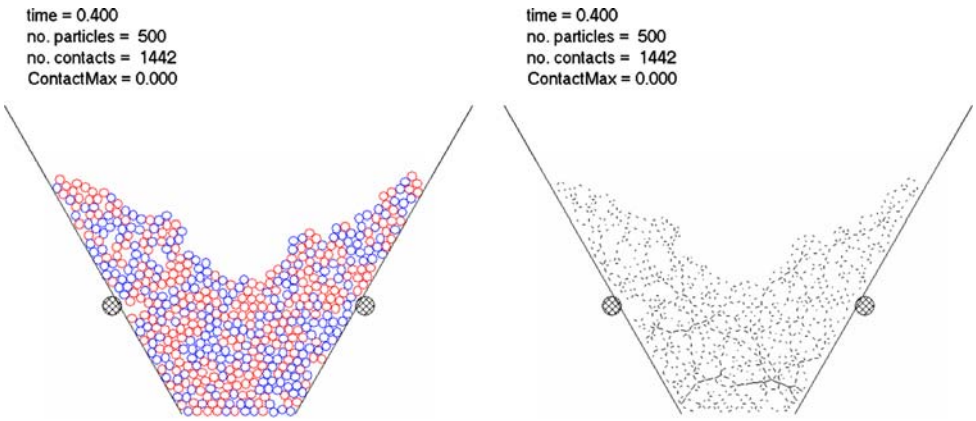

Fig. 8 Two-dimensional simulation: particle positions and contact forces at end of simulation for $B = 12D$, $h = 12D$, $f = 90$ Hz, showing negligible discharge

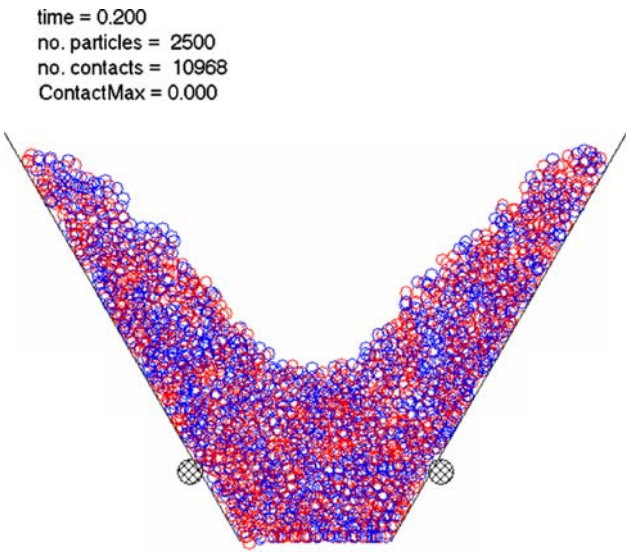

Fig. 9 Three-dimensional simulation: particle positions at end of fill for $B = 12D$, $k_{na} = 250$ dyne/cm, showing effect of "higher cohesion" in 3D—high slopes on free surface—no discharge on vibration (All particles drawn)

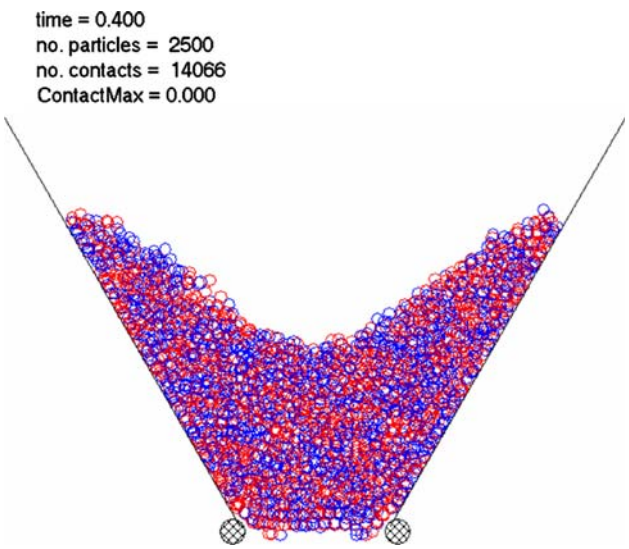

Fig. 10 Three-dimensional simulation: particle positions at end of simulation for $B = 12D$, $k_{na} = 90$ dyne/cm, $h = 0D$, $f = 70$ Hz, showing negligible discharge

the same in both cases here, so effectively the surface force to weight ratio is higher in 3D. Friction from the front and back (cohesionless) planar walls is probably also a factor

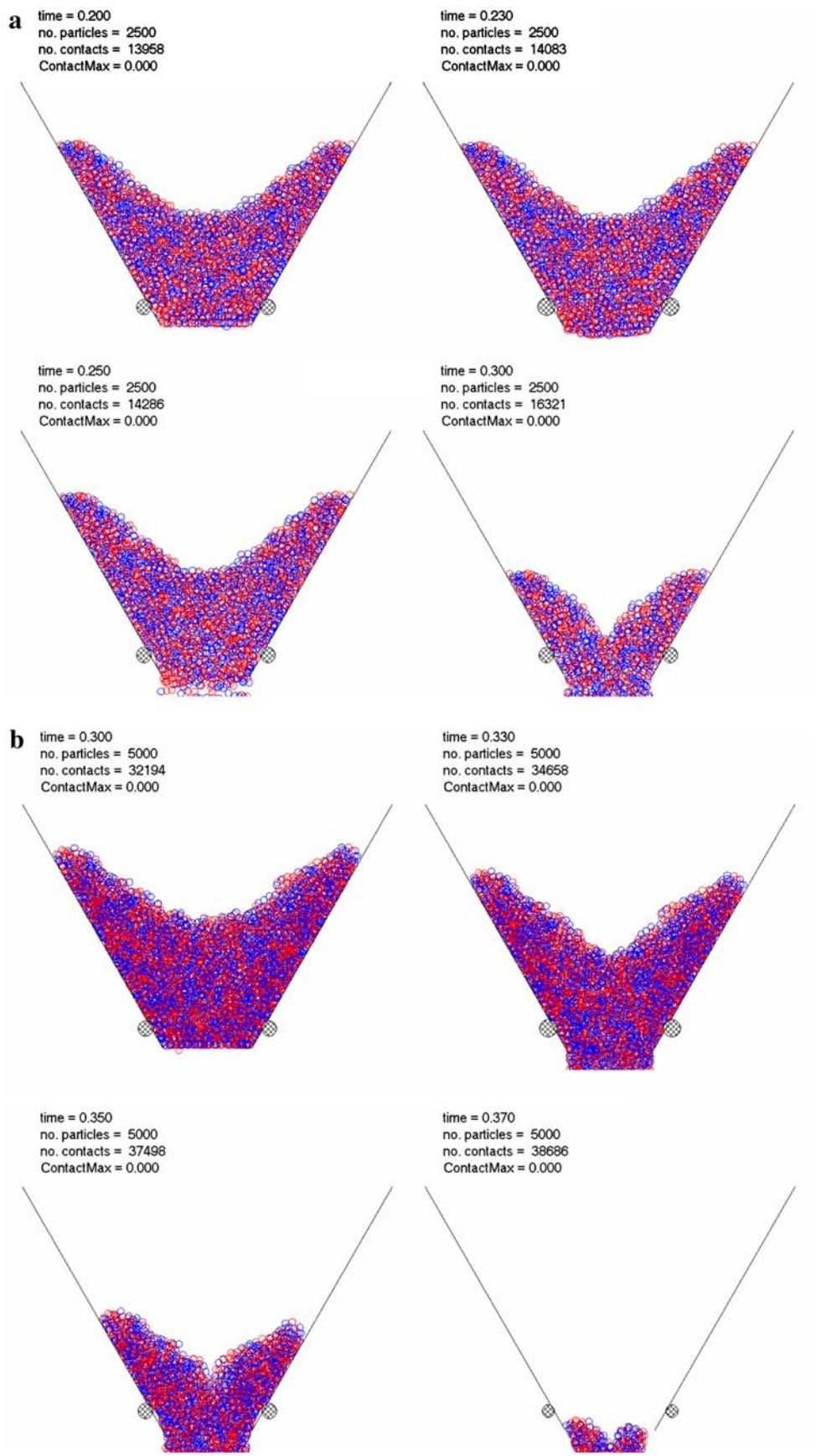

Fig. 11 **a** Three-dimensional simulation: particle positions during discharge for $B = 12D$, $k_{na} = 90$ dyne/cm, $h = 3D$, $f = 70$ Hz. Vibration start at $t = 0.2$ s, fully discharged by $t = 0.32$ s; **b** 3D simulation: particle positions during discharge for same data as **a** except $N = 5,000$, $W = 10D$. Vibration start at $t = 0.3$ s, fully discharged by $t = 0.38$ s

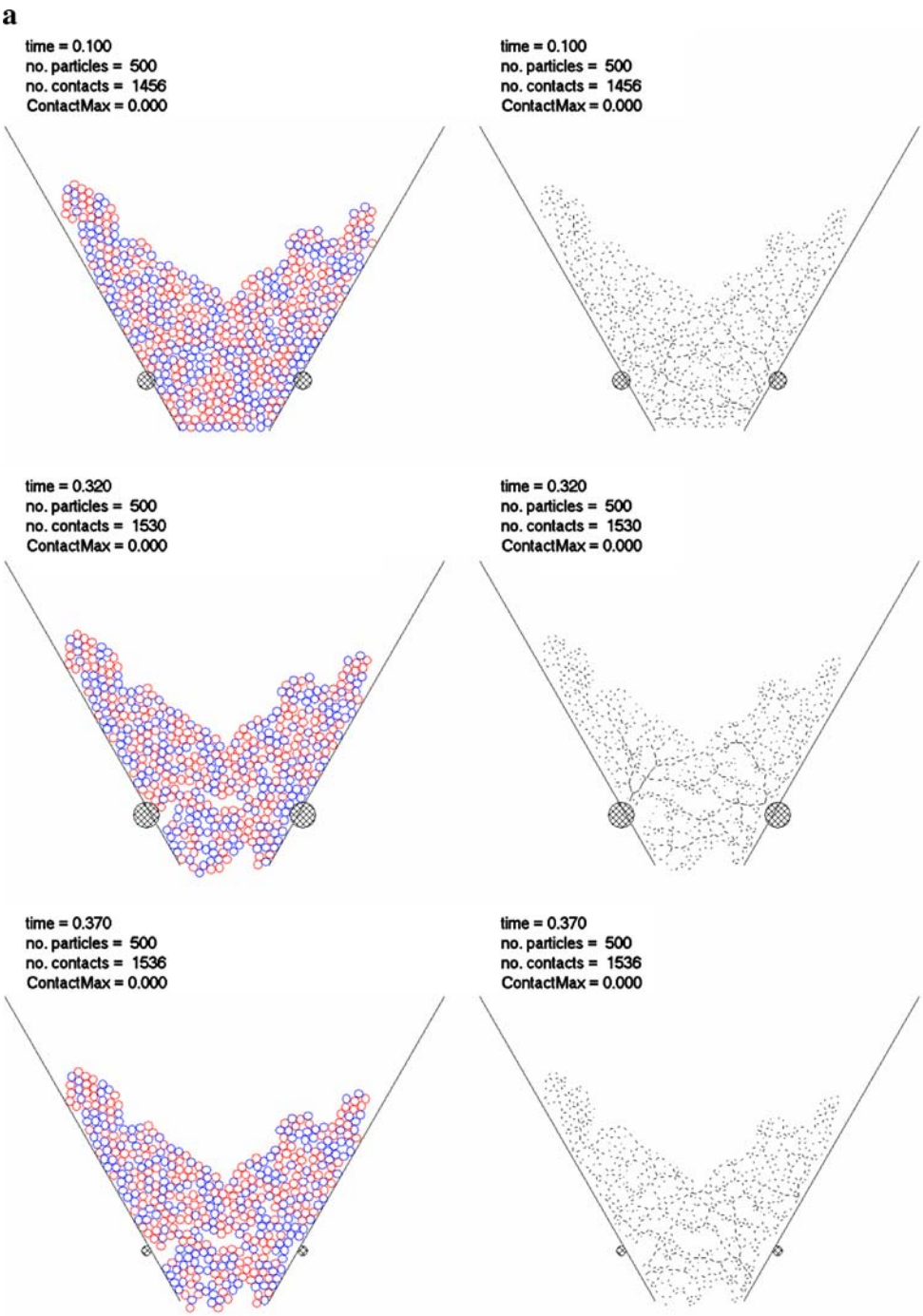

Fig. 12 **a** Two-dimensional simulation: snapshots of particle positions and contact forces for $B = 10D$, $h = 6D$, $A = 0.5D$—partial discharge at $t = 0.4$ s; **b** 2D simulation: snapshots of particle positions and contact forces for $B = 10D$, $h = 6D$, $A = 1.0D$—total discharge at $t = 0.23$ s

here. Figure 9 shows the case of a filled hopper. The slope of the material free surface is significantly higher than in the 2D equivalent case, indicative of higher cohesion. Consequently the material did not flow even under high vibration frequency. Some further simulations were used to gauge the value of k_{na}, the cohesive stiffness, which gives similar flow as in the 2D cases. This value is about 90 dyne/cm, reduced from 250 for the 2D.

Figure 10 shows a case where the vibration point $h = 0$ was too low. A similar figure (not shown) was obtained for $h = 6D$. Figure 11a shows the case for the same data but $h = 3D$ where total discharge occurred. This case was repeated in Fig. 11b for a larger depth of hopper and more particles. The flow here was somewhat faster indicating the front and back walls have some effect, but that the type of flow is similar.

In summary, the 3D simulations showed overall similar fill, flow and response to vibration as the 2D simulations, except that the cohesive forces needed to be reduced due to the higher co-ordination number.

Fig. 12 continued

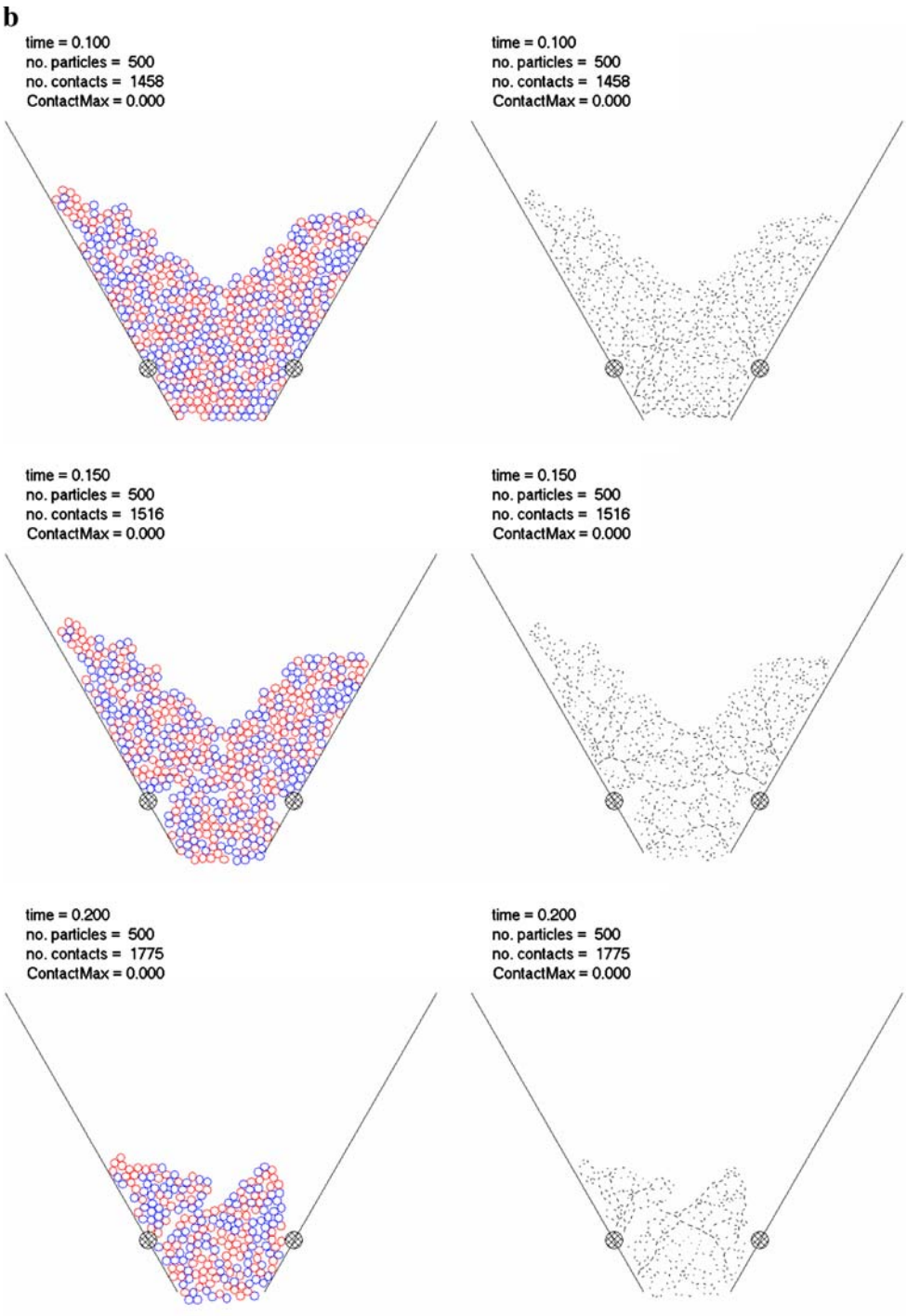

4.3 Large amplitude low frequency in 2D

This section investigates the concept of using a low frequency but high amplitude to essentially "push" the material out. The mechanism here is somewhat different to Sect. 4.1 which looked at transmitting vibration to break particle bonds and hence arches from localised point source vibration.

A frequency of 10 Hz was chosen to allow sufficient movement within $t = 0.1$ to 0.4 s and for which the speed of vibrator motion is comparable with the speed of the particles when filling the hopper, ie not excessive. The question here is what size of vibrator and what amplitude is required to enable flow. (In Sect. 4.1 $R_{\text{vib}} = 1D$, $A = 0.3D$.)

Taking as a starting point $B = 10D$, $h = 6D$ it was found that amplitude A in the range 0.5–0.85D gave a partial discharge and $A = 1D$ enabled total discharge as shown in Fig. 12. This indicates that even with the low frequency a large enough amplitude can discharge the material. Testing

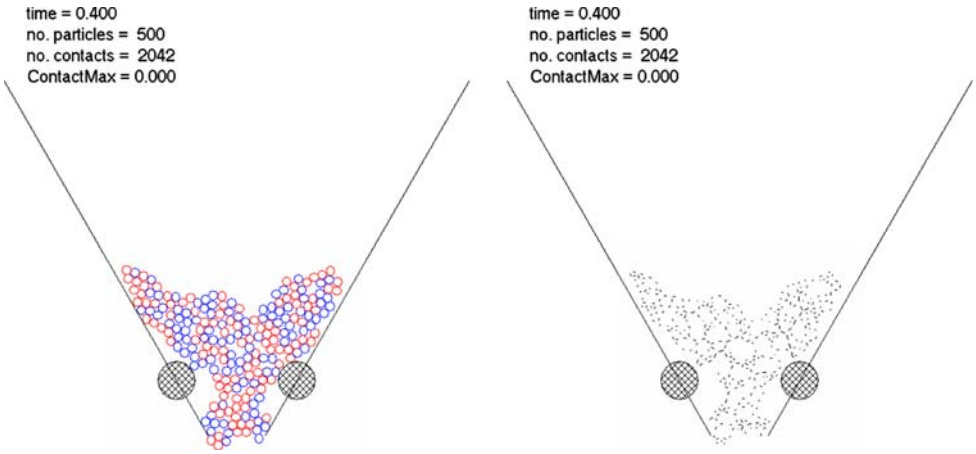

Fig. 13 Particle positions and contact forces for $B = 6D$, $h = 6D$, $A = 2.0D$ showing most particles discharged at $t = 0.4$ s

this further B was reduced to $6D$(h and f constant). This is clearly a challenging case. With $A = 1D$ there was minimal flow although the region around the vibrators was clear. With an increase to $A = 2D$ (with a larger vibrator circle $R_{\text{vib}} = 2D$) the material has mostly discharged by $t = 0.4$ s—see Fig. 13. The cohesive nature of the particles is evident from the form it takes up. Essentially it is being pushed out en masse like dough. As noted, there is no particle-wall cohesion here. That would be a more challenging situation. It is significant that the residual, cohesive arch in Fig. 13 has formed below the location of the vibration, and a tendency to a passive stress state is indicated.

5 Conclusions and future work

This paper investigates the use of vibration to promote flow of cohesive granular material in wedge-shaped hoppers. It compares a continuum and discrete element approach.

It is shown that despite the obvious limitation of computer runtime requirements in DEM the discrete model can be scaled to illustrate significant physical phenomena. Continuum models have the advantage that they can model the full-scale system, however, the models can be complex and require significant assumptions. DEM can be fairly simple at the particle level, but significant runtime is required. This paper illustrates how the techniques can be used in tandem to enhance the overall picture.

The results here show that the DEM model agrees in principle with the Stress Arc continuum approach. If the vibration source is located too near the orifice or if it is located too high it will not be at maximum effectiveness. For one hopper with a small orifice modelled there was only a small region in which the vibration could be placed to enable flow. Investigation of contact forces in the model indicated that during vibration discharge the stress state was in passive mode at the vibrator position, tending more to the active state above and dilated below. This is supportive of the continuum model assumptions. Most DEM simulations were undertaken in 2D. The 3D simulations supported the general trends, showing similar behaviour, except that the cohesiveness was enhanced.

Low frequency high amplitude vibration was also shown to be able to discharge through quite small orifices (2D study). The nature of vibration is somewhat different here. At higher frequency low amplitude it tends to break the cohesive arch; at the lower frequency high amplitude it is effectively displacing the material.

There is considerable scope for future work here. This could include comparisons with laboratory experiments, measurement of internal stresses and simulation of non-spherical particles. It is envisaged that the latter could be important in that vibration might align them, increasing the area of contact and hence increase cohesion. It is also speculated that possibly some form of "intelligent vibration" might be worth investigating. That is the vibration at a series of sources could change (frequency, amplitude, shape, co-ordination) dependent on the response of material in the hopper.

Acknowledgments We are grateful to the reviewers for some useful suggestions, in particular relating to Eqs. 5, 10, and 11 and Sects. 3.3 and 4.2.

References

1. Jenike, A.W.: Quantitative design of mass-flow bins. Powder Technol. **1**(4), 237–244 (1967)
2. Enstad, G.: On the theory of arching in mass flow hoppers. Chem. Eng. Sci. **30**, 1273–1283 (1975)
3. Williams, J.C.: The rate of discharge of coarse granular materials from conical mass flow hoppers. Chem. Eng. Sci. **32**, 247–255 (1977)
4. Langston, P.A., Nikitidis, M.S., Tuzun, U., Heyes, D.M., Spyrou, N.M.: Microstructural simulation and imaging of gran-

ular flows in two- and three-dimensional hoppers. Powder Technol. **94**(1), 59–72 (1997)
5. Kozichi, J., Tejchman, J.: Application of a cellular automation to simulations of granular flow in silos. Granular Matter **7**, 45–54 (2005)
6. Kamath, S., Puri, V.M., Manbeck, H.B., Hogg, R.: Flow properties of powders using four testers—measurement, comparison and assessment. Powder Technol. **76**(3), 277–289 (1993)
7. Arnold, P.C.: Flow properties for mass-flow hopper geometry determinations—what range of shear testing is required. Powder Handling Process **15**(5), 315–317 (2003)
8. IMechE conference, Hopper & Silo Discharge: Successful Solutions, IMechE, London, 27 November (1998)
9. Bradley, M.: Strategy for Selecting Solutions, paper 13, Hopper & Silo Discharge: Successful Solutions, IMechE, London, 27 November (1998)
10. Roberts, A.W.: Chapter 5. In: Fayed, M.E., Otten, L. (eds.) Handbook of Powder Science and Technology, 2nd edn. Chapman & Hall, New York (1997)
11. Matsusaka, S., Urakawa, M., Masuda, H.: Micro-feeding of a fine powder using a capillary tube with ultrasionic vibration. Adv. Powder Technol. **6**(4), 283–293 (1995)
12. Matsusaka, S., Yamamoto, K., Hiraoki, H.: Micro-feeding of a fine powder using a vibrating capillary tube. Adv. Powder Technol. **7**(2), 141–151 (1996)
13. Matsusaka, S., Urakawa, M., Furutate, M., Masuda, H.: Micro-feeding of fine powders using a capillary with ultrasonic vibration. In: Third World Congress on Particle Technology, paper 343, Brighton, England, June (1998)
14. Matchett, A.J.: A theoretical model of vibrationally induced flow in conical hopper systems. Chem. Eng. Res. Des. **82**(A1), 85–98 (2004)
15. Walker, D.M.: An approximate theory for pressure and arching in hoppers. Chem. Eng. Sci. **21**, 975–997 (1966)
16. Walters, K.: A theoretical analysis of stresses in silos with vertical walls. Chem. Eng. Sci. **28**, 13–21 (1973)
17. Asmar, B.N., Langston, P.A., Matchett, A.J., Walters, J.K.: Validation tests on a distinct element model of vibrating cohesive particle systems. Comput. Chem. Eng. **26**(6), 785–802 (2002)
18. Fraige, F., Langston, P.A.: Integration schemes and damping algorithms in distinct element models. Adv. Powder Technol. **15**(2), 227–246 (2004)
19. Li, J., Langston, P.A., Webb, C., Dyakowski, T.: Flow of sphero-disc particles in rectangular hoppers—a DEM and experimental comparison in 3D. Chem. Eng. Sci. **59**(24), 5917–5929 (2004)
20. Fraige, F.Y., Langston, P.A., Chen, G.Z.: Distinct element modelling of cubic particle packing and flow. Powder Technol. (in press)
21. Joseph Anthony, S., Hoyle, W., Ding, Y. (eds.) Review of Granular Materials—Fundamentals and Applications, The Royal Society of Chemistry, Cambridge (2004)
22. Langston, P.A., Heyes, D.M., Tüzün, U.: Discrete element simulation of granular flow in 2D and 3D hoppers: dependence of discharge rate and wall stress on particle interactions. Chem. Eng. Sci. **50**, 967 (1995)
23. Yang, R.Y., Jayasundara, C.T., Yu, A.B., Curry, D.: DEM simulation of the flow of grinding media in IsaMill. Miner. Eng. **19**, 984–994 (2006)
24. Nedderman, R.M.: Statics and kinematics of granular materials. Cambridge University Press, Cambridge (1992)